ZDES Simulation and Spectral Analysis of a High-Reynolds-Number Out-of-Equilibrium Turbulent Boundary Layer

Jaime Vaquero, Nicolas Renard, Sébastien Deck

ZDES simulation and spectral analysis of a high-Reynolds-number out-of-equilibrium turbulent boundary layer

Jaime Vaquero[1*], Nicolas Renard[1] and Sébastien Deck[1]

[1*]ONERA,The French Aerospace Lab, 8, Rue des Vertugadins, F-92190, Meudon, France.

*Corresponding author(s). E-mail(s): jaime.vaquero@onera.fr;
Contributing authors: nicolas.renard@onera.fr;
sebastien.deck@onera.fr;

Abstract

A test-case for the assessment of Zonal Detached Eddy Simulation (ZDES) mode 3 (which corresponds to a Wall-Modelled Large Eddy Simulation approach, WMLES) for turbulent boundary layers in pressure gradient conditions is presented. The demanding test-case corresponds to an experiment at high Reynolds number, reaching up to $\boldsymbol{Re_\theta \approx 13000}$, probably too expensive for DNS (Direct Numerical Simulation) or WRLES (Wall-Resolved Large Eddy Simulation), but still affordable using ZDES mode 3 (WMLES). At the considered station, the boundary layer is in out-of-equilibrium conditions. The presented results prove the advantage of the scale-resolving approach, the ZDES mode 3, with respect to the RANS approach, as evidenced by the better representation observed for the mean velocity and Reynolds stress profiles, in particular in the outer layer where non-canonical effects are more evident. Thanks to the resolved turbulence, a more physically realistic flow is predicted by ZDES mode 3 and more in depth analysis of turbulence is accessible. In particular, spectral analysis of turbulence is performed in this study, and a scale-dependent convection velocity is also assessed for the first time with a hybrid RANS/LES approach in out-of-equilibrium conditions. Such analysis allow to identify some features of the turbulent scales distribution within the boundary layer, which seem responsible for some uncommon features observed in the present mean flow.

Keywords: Wall turbulence, ZDES simulation, Hybrid RANS/LES, Out-of-equilibrium flows, Spectral analysis

1 Introduction

The scientific community of turbulence research is devoting important efforts to the study of pressure gradients effects on turbulent boundary layers and separation. A better understanding of these would lead to a significant improvement of performance in many industrial devices. Nowadays, numerical simulations are essential in fluid mechanics research and broaden the research possibilities by complementing experimental studies. However, when considering turbulence numerical simulations there are still important practical limitations.

A turbulent flow exhibits a wide range of turbulent scales and the separation between the smallest ones and the largest ones increases when so does the Reynolds number [1, 2]. At typical Reynolds number of industrial applications, the separation of scales is so important that directly solving all the flow structures (which corresponds to the Direct Numerical Simulation approach, DNS) requires extremely fine meshes that, together with the huge number of time steps for statistical convergence of the mean flow, results in non-affordable simulations despite the most advanced high performance computational resources. In particular, in the test-case presented later in this work [3], a DNS would require at the considered Reynolds number around $N_{xyz} = 50 \times 10^9$ points whereas the approach used in the present work needs about $N_{xyz} = 46 \times 10^6$. The given values for DNS and WRLES are estimated according to classical grid requirements for wall-bounded turbulent flows, as for instance in [2, 4, 5]. This example illustrates why avoiding solving some (or all) of the turbulent scales is a widely used alternative.

Reynolds-Averaged Navier Stokes (RANS) equations allow to solve the mean field and require a closure for the Reynolds stress term in the momentum equation. This is known as RANS approach. Another approach extensively used is the Large Eddy Simulation (LES) which aims at solving only the energetic scales, and modelling the dissipative (small) scales by means of a subgrid-scale model (SGS model). Nevertheless, in wall-bounded turbulent flows, the relaxation in the mesh size is not very important between Wall-Resolved LES (WRLES) and DNS [6], because of the dependence of the energetic scales size with the wall distance. A bigger reduction of the computational effort may be obtained by modeling the near wall region of the boundary layer using an approach called Wall-Modelled LES (WMLES) in contrast to WRLES. Such approach allows to decrease the number of points in the inner region of the boundary layer resulting in a significant lessening of the total number of points [6, 7]. Indeed, according to [6], the number of points needed for the simulation of turbulent boundary layers increases as $N_{xyz} \sim Re_\theta^{2.4}$ for

a DNS, $N_{xyz} \sim Re_\theta^{2.17}$ for a WRLES and $N_{xyz} \sim Re_\theta^{1.17}$ for a WMLES, where Re_θ is the Reynolds number based on the momentum thickness θ. In other words, higher Reynolds numbers at an affordable cost are achievable by means of WMLES, compared to WRLES or DNS.

Among the different stategies of using WMLES (which are not discussed in this work), the mode 3 of the Zonal Detached Eddy Simulation approach (ZDES) [8] is used in this study, which is a hybrid RANS/LES approach and has been validated for zero-pressure-gradient turbulent boundary layers at high Reynolds numbers [6, 9, 10]. It is important to mention that ZDES mode 3 may also be employed as a WRLES approach, as done in the work of Deck *et al.* [11].

Most studies related to pressure gradient boundary layers or turbulent boundary layer separation are performed either experimentally or numerically using DNS or WRLES [12–19]. However, due to the computational cost, numerical studies are in general limited in terms of Reynolds number even for recent works (see for instance [20–23]). The main contribution of the present work is the numerical study and spectral analysis of turbulence of a high-Reynolds-number turbulent boundary layer in pressure gradient conditions thanks to the hybrid RANS/LES approach ZDES, and more specifically the ZDES mode 3 (WMLES approach). The Reynolds number in the present simulation is large enough to illustrate in terms of computational effort the interest of the ZDES mode 3, which is again proved in the results obtained.

This manuscript is structured as follows. First, the turbulence modelling techniques employed in the present work are introduced and in particular the ZDES mode 3 is detailed, in section 2, followed by some comments regarding the turbulent inflow conditions and numerical aspects as well. Then, section 3 presents the test-case devoted to the effects of pressure gradients, followed by the results discussion, which is based on different levels of turbulent flow analysis, mainly the instantaneous field, the mean field, a spectral analysis of turbulence and the assessment of a scale-dependent convection velocity. Finally, the last section of the manuscript is devoted to the conclusions of the present work.

2 Turbulence modelling

2.1 RANS models

In order to study the capabilities of RANS modelling for predicting pressure gradient turbulent boundary layer flows, several RANS models of different levels of complexity are considered in the present study, mainly the Spalart-Allmaras [24], the $k-\omega$ Menter SST [25] (which are eddy-viscosity models) and the Reynolds Stress Model (RSM) SSG-LRR-ω [26–28]. Eddy-viscosity models rely on a closure used to link the Reynolds stress tensor to the mean flow variables. This closure is in many cases (but not always) given by the

Boussinesq's hypothesis which in an incompressible case reads [1, 29]:

$$\begin{aligned} -\rho\langle u_i' u_j'\rangle &= 2\mu_t\langle S_{ij}\rangle - \frac{2}{3}\rho k\delta_{ij}, \\ \langle S_{ij}\rangle &= \frac{1}{2}\left(\frac{\partial\langle u_i\rangle}{\partial x_j} + \frac{\partial\langle u_j\rangle}{\partial x_i}\right) \end{aligned} \tag{1}$$

where $\langle\bullet\rangle$ denotes Reynolds average, ρ is the fluid density, u_i' is the i^{th} component of the fluctuating velocity, μ_t the eddy viscosity, k the turbulent kinetic energy and δ_{ij} the Kronecker delta (tensor). In the case of second order models, the transport equation for the Reynolds stresses is considered [1]:

$$\frac{\partial}{\partial t}\langle u_i' u_j'\rangle + \langle u_l\rangle\frac{\partial}{\partial x_l}\langle u_i' u_j'\rangle = \mathcal{P}_{ij} + \mathcal{R}_{ij} - \frac{\partial}{\partial x_l}\mathcal{T}_{lij} - \varepsilon_{ij}. \tag{2}$$

Due to the symmetry of the Reynolds stress tensor, the additional number of equations to solve is one for each Reynolds stress component (which makes 6) and an additional one for a given turbulent variable, which may be the turbulent kinetic energy dissipation rate ε or the specific dissipation rate ω [1]. In equation (2), $\mathcal{P}_{ij}$ is the production tensor, $\mathcal{R}_{ij}$ is the pressure-rate-of-strain tensor, $\mathcal{T}_{lij}$ the Reynolds stress flux and ε_{ij} the dissipation tensor. In this case, the production tensor and the viscous diffusion tensor (included in $\mathcal{T}_{lij}$) are completely solved since both the mean flow and the Reynolds stress are accessible. However, the remaining terms in equation (2) need to be modelled [1, 29]. Details of the RSM model employed in this work may be found in [26–28].

2.2 ZDES mode 3

The Zonal Detached Eddy Simulation (ZDES) is a hybrid RANS/LES approach developed since the early 2000s that allows to treat a given problem by means of three different operating modes depending on the flow configuration as described in [8]. Among the three modes, the mode 3 is used in the present study since it corresponds to a WMLES approach that has been employed in several studies [6, 9, 10, 30] and it may also be used for WRLES as in [11]. A detailed description of the method is presented in the following.

The mode 3 of the ZDES uses the Spalart-Allmaras turbulence model [24]. In the inner part of the boundary layer, a RANS approach is performed whereas in the outer part and outside the boundary layer a LES approach is used. The same turbulence model is used both for RANS and as a SGS model for LES because the Spalart-Allmaras model shows a behaviour similar to the Smagorinski's SGS model [31] when equilibrium conditions are considered. Indeed, when the length scale of the model (which corresponds to the wall distance d_w) is replaced by $C_{\text{DES}}\Delta$ (being C_{DES} a constant and Δ the LES filter width), assuming an equilibrium between production and destruction of

$\nu_t = \mu_t/\rho$ leads to $\nu_t \sim S\Delta^2$, where S corresponds to the local strain rate [2, 8, 32].

The separation between the RANS region and the LES region is given by an interface (in particular by its wall distance d_w^{int}) which is explicitly provided by the user. The characteristic length of the turbulence model $\tilde{d}_{\text{ZDES}}^{\text{III}}$, once the position of the interface defined, is given by:

$$\tilde{d}_{\text{ZDES}}^{\text{III}} = \begin{cases} d_w & \text{if } d_w < d_w^{\text{int}} \\ \min(d_w, C_{\text{DES}}\Delta_{\text{vol}}) & \text{if } d_w \geq d_w^{\text{int}} \end{cases} \tag{3}$$

where $C_{\text{DES}} = 0.65$ and $\Delta_{\text{vol}} = \mathcal{V}^{1/3}$ being $\mathcal{V}$ the cell volume. Other slight modifications of the model are also made for a proper behavior and the reader may find them in [8]. Besides, a recent improvement of the method has been made by [33] which softens the binary transition from RANS to LES near the RANS/LES interface leading to a better friction coefficient prediction thanks to a continuous function f_δ. This function, which ranges from 0 to 1 and provides also continuous derivatives, is included in the new expression of $\tilde{d}_{\text{ZDES}}^{\text{III}}$:

$$\tilde{d}_{\text{ZDES}}^{\text{III}} = (1 - f_\delta) \cdot d_w + f_\delta \cdot \min\left(d_w, C_{\text{DES}}\Delta_{\text{vol}}\right) \tag{4}$$

and is written as follows:

$$f_\delta(\alpha) = \begin{cases} 0 & \text{si} \quad \alpha \leq -1 \\ \dfrac{1}{1 + \exp\left(\dfrac{-6\alpha}{1-\alpha^2}\right)} & \text{si} \quad -1 < \alpha < 1 \\ 1 & \text{si} \quad \alpha \geq 1 \end{cases}.$$

Here α is a parameter defined for each mesh cell j as :

$$\alpha(j) = \frac{d_w(j) - d_w^{\text{int}}(x)}{0.1 d_w^{\text{int}}(x)}. \tag{5}$$

The f_δ function is also employed for the switch of the Spalart-Allmaras model functions which in the LES region are set to $f_{v1} = 1$, $f_{v2} = 0$ and $f_w = 1$ [8, 10].

2.3 Inflow boundary conditions and history effects

Numerical simulations in which turbulence is either partially or totally resolved, as in the case of ZDES mode 3, require turbulent inflow conditions. Among the several ways to introduce turbulence in a computational domain (see [10]), the Synthetic Eddy Method (SEM) [34, 35] is considered in the present study, after the modifications introduced by [30, 36] for its application in ZDES mode 3 simulations, already employed in other studies such as [3, 6, 9, 10, 37]. Briefly, the idea consists in injecting fluctuations of the velocity

field to a mean flow that are intended to mimic turbulent fluctuations. This is achieved by using a Cholesky decomposition of the Reynolds stress tensor, and a velocity fluctuation obtained from criteria aiming at reproducing the length and velocity scales of turbulent fluctuations dependent on the wall distance. Despite the efforts to mimic turbulent fluctuations features, the fluctuations introduced are not perfectly realistic and they require some amount of time (and therefore convection in the computational domain) until they become proper turbulent fluctuations of the problem studied.

The behavior of SEM for studies of zero-pressure-gradient turbulent boundary layers is very satisfactory [10]. The rich literature on the effects of upstream perturbations on turbulent boundary layers draws a complex picture when it comes to adverse pressure gradient conditions. A recent study by the authors aimed to identify whether disturbances of the boundary layer in such conditions would eventually disappear or, conversely, increase [38]. The results show that convergence to a reference state requires important distances of the order of 10^4 and 10^2 times the initial boundary layer thickness for laminar and turbulent boundary layers respectively. Besides, it was observed that for all of the favorable pressure gradient cases and the moderate adverse pressure gradient ones, convergence was always obtained. Therefore, this is a satisfactory result that allows to use the unsteady boundary conditions in the same way as for previous zero-pressure-gradient studies [10] since the possible defects of the inflow condition will gradually vanish after a sufficiently long convection distance.

2.4 Numerical methods

Different modelling approaches are presented in this work, for which the suitable numerical methods are not the same. Differences exist in particular between RANS simulations (either eddy-viscosity or Reynolds stress models) and ZDES simulations. Indeed the flow solved is intrinsically dissimilar between both approaches and the numerical methods adapted for one are not the same as those for the other.

In the case of RANS simulations, the finite volume method with Roe's scheme is considered for spatial discretization together with a MUSCL approach (Monotonic Upstream Scheme for Conservation Laws) for flux reconstruction at the cell faces. A pseudotemporal integration is done by virtue of an implicit Euler's scheme. Simulations with the Spalart-Allmaras model are made using the in-house research solver FLU3M [39] developed at ONERA, and those using the $k-\omega$ Menter SST model and the RSM model are made with the ONERA industrial solver *elsA* [40]. In order to avoid uncertainty in the results obtained coming from the fact of using different solvers, comparisons between the solutions provided by the two solvers using the Spalart-Allmaras model and the same numerical schemes have been made (not shown) giving a perfect agreement.

Regarding the ZDES approach, simulations are performed with the solver FLU3M. This solver has already been used in previous studies for high fidelity

simulations [6, 8, 10, 11, 30]. The definition of the numerical methods employed is slightly more complex. In fact, due to the zonal feature of the method, the ZDES mode 3 is considered only for the boundary layer of interest, which is the one developing over the bottom wall (in which experimental measurements have been recorded in the test-case [41]). At the top wall a full unsteady RANS approach (URANS) with the Spalart-Allmaras model is retained. Thus, modelling effects are only impacting the boundary layer of interest when comparing to full RANS simulations. Besides, this is the reason why in figure 2 turbulent structures in the schlieren contour are solely observable in the bottom-wall boundary layer. This illustrates the asset of ZDES to focus only on the region of interest while resorting to RANS (mode 0 of ZDES) for the rest of the flow at a reduced computational cost, contrary to typical full WMLES strategies. In the (approximate) bottom half domain, where the ZDES mode 3 is applied, the spatial scheme is the AUSM + (P) (proposed by [42] and modified as in [43] for dissipation reduction purposes). In the upper domain, the AUSM + (P) scheme is employed (without the modification of [43]), contrary to Roe's scheme used in full RANS simulations. The reason for this change is based on numerical schemes compatibility between the ZDES mode 3 region and the RANS region in that same simulation.

3 Description of the problem studied

The experimental work of [41] (for the lowest free stream velocity) has been chosen for numerical reproduction due to several aspects. On the one hand, the Reynolds number of the problem is representative of applied aerodynamics problems where hybrid RANS/LES approaches are suitable because the numerical effort for a DNS or WRLES would be excessive. Indeed, reaching this Reynolds number of $Re_\theta \approx 13000$ (where θ is the boundary layer momentum thickness) would require about 50×10^9 and 3×10^9 grid points respectively for DNS and WRLES. In the case of ZDES mode 3 instead, the number of mesh points is significantly reduced down to 46×10^6 (around a thousand and a hundred times less points respectively). Given the computational cost of such simulations, some decisions have been made to decrease the number of points as much as possible. In particular, the side-walls boundary layers are not solved (and periodicity is imposed in the spanwise boundaries) but their contraction effect (which is non-negligible due to the thickness of the boundary layer with respect to the span of the wind tunnel) is taken into account by means of a modification of the top wall geometry as detailed in [3]. This gives a good match of the simulated pressure coefficient with the experimental values [3].

A view of the computational domain for the ZDES simulation is presented in figure 2 in which the flow goes from left to right and the mesh resolution is taken as $\Delta x^+ = 200$, $\Delta z^+ = 100$ and $\Delta y_w^+ = 1$ (the symbol '+'refers to viscous scales and the subscript 'w' refers to the wall). In the case of the RANS simulations, the mesh spacings are the same and the only difference is that the inlet of the domain is placed farther upstream. More precisely, for the

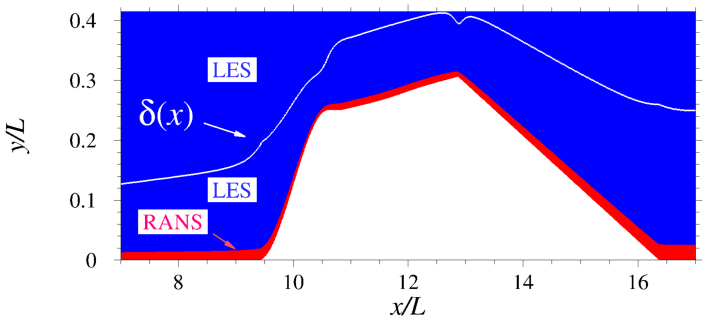

Fig. 1 Position of the RANS/LES interface. RANS approach is applied in the red area and LES in the blue area. The vertical axis is magnified for clarity purposes.

latter the inlet is placed at $x/L = -2.01$ whereas in the ZDES computation it is placed at $x/L = 6.6$, where L is the real height of the wind tunnel. It is reminded that for the ZDES simulation, unsteady boundary conditions (SEM) are used which already give a boundary layer profile at the inlet and therefore this allows to place the inlet farther downstream than in RANS computations where the boundary layer develops from a uniform inlet boundary condition. Besides, as stated in section 2.3 the SEM requires a boundary layer profile that is obtained from a RANS solution, which is the reason why the computational domain is longer in RANS simulations.

For the ZDES mode 3 simulation, the RANS/LES interface is placed at a wall distance $d_w^{\text{int}} = 0.1\delta$ (see figure 1) where δ is the boundary layer thickness defined as $\langle u \rangle_{(y=\delta)} = 0.99U_e$, being U_e the external streamwise velocity. Such a positionning of the interface results in applying the RANS approach to the inner layer of the boundary layer in the LES approach to the outer layer. Due to the curvature and pressure gradients effects experienced by the boundary layer, a method for the boundary layer edge detection relying on the local mean spanwise vorticity profile is employed. This method is based on the suggestion of [12] for the definition of the external velocity from the mean vorticity, also employed for instance in [16]. In the present work, as in [3], the complete spanwise vorticity is considered, and the external velocity is obtained as the streamwise mean velocity at a position where the mean vorticity (in the spanwise direction) is equal to a fraction of the wall mean vorticity given by a threshold of about 2×10^{-4}.

4 Results

4.1 Instantaneous field

The instantaneous field obtained from the ZDES mode 3 simulation is presented at first. Figure 2 shows an isosurface of Q-criterion [44] together with a numerical schlieren (norm of density gradient). As observed in this figure, an

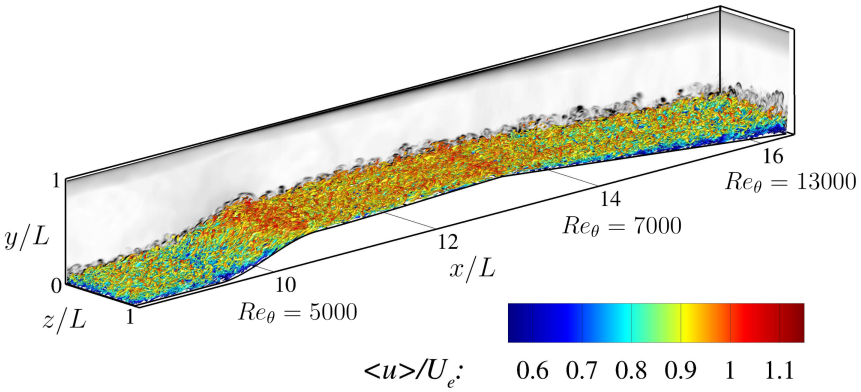

Fig. 2 Isosurface of the Q-criterion for $Q = 0.14\,(U_0/\delta_0)^2$ together with numerical schlieren contours, being U_0 and δ_0 the streamwise free stream velocity and the boundary layer thickness at the inlet. Values of the Reynolds number based on the momentum thickness are given at stations $x/L = 10,\ 14$ and 16.

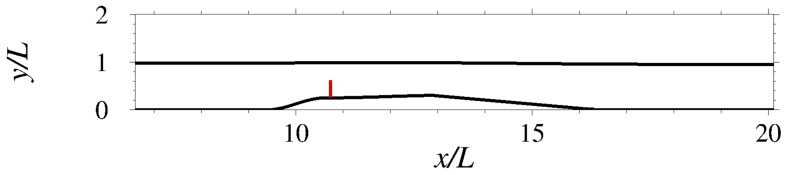

Fig. 3 Location of the station $x/L = 10.73$, indicated by the red mark.

important part of turbulence in the boundary layer is resolved and the hairpin type structure is observable which is a typical structure found in turbulent boundary layers [45]. As already mentioned in a previous section, the schlieren contours do not show any turbulent fluctuation in the upper boundary layer due to the zonal feature of the ZDES approach allowing to use a full RANS strategy for this boundary layer. However, a smooth gradient is still observable resulting from temperature increase as a consequence of friction losses.

4.2 Mean field

Profiles of the mean velocity and the Reynolds shear stress are presented in figures 4 and 5 respectively for all the models considered (Spalart-Allmaras, $k-\omega$ Menter SST, SSG-LRR-ω and ZDES mode 3) at $x/L = 10.73$ (see figure 3). This station is placed right upstream of the favorable-pressure-gradient flat plate and it is chosen due to the unusual shape of the profiles compared to those of zero-pressure-gradient turbulent boundary layers. Indeed, the experimental data shows a velocity excess in the mean velocity profile at $y = 0.15\delta$ as well as an external peak in the Reynolds shear stress profile. It is observed that, among the models presented, the Spalart-Allmaras is the least accurate, particularly in the near wall region for both the mean velocity and Reynolds

shear stress profiles and is also not able to reproduce the external peak in the latter. Better results, yet perfectible, are given by the $k-\omega$ Menter SST model which also misses the external peak of the Reynolds shear stress, but improves considerably the mean velocity profile prediction. The RSM model is more accurate in the mean velocity profile and is able to predict the external peak of the Reynolds shear stress as well, although the levels of this peak are underestimated compared to the experimental measurements. Besides, the outer peak is considerably narrower than in the experiment. The shape of the Reynolds shear stress profile as well as its levels are better represented by the ZDES mode 3 which is also able to properly reproduce the mean velocity excess observed experimentally around $y = 0.15\delta$, thus suggesting that the non canonical features of the flow at this particular station are better taken into account by the resolved turbulence.

In addition, figure 6 illustrates the profiles of u_{rms} and v_{rms} for both ZDES mode 3 and the DRSM model. Eddy-viscosity models are absent in this figure since normal Reynolds stresses are not provided by the Spalart-Allmaras nor the $k-\omega$ Menter SST models. These figures are given in linear representation because the focus is made on the outer layer. Indeed, the inner part of the ZDES mode 3 (shaded in grey in the figure) is treated in RANS and therefore comparisons of these quantities for ZDES mode 3 in the inner region are not pertinent because u_{rms} and v_{rms} are not provided by the RANS approach considered in the method. The DRSM model gives a fairly accurate estimation of the Reynolds normal stresses, although in the inner region there is an underestimation of u_{rms} and the contrary is observed for v_{rms}. The underestimation of u_{rms} is not surprising since the DRSM model considered lacks of near wall treatment [28, 46]. In the outer layer it is observed a general trend to slightly underestimate the levels of the normal stresses. Results from ZDES mode 3 in the outer layer seem to be a bit closer to the levels of the experimental measurements, and better agreement is also observed in the trend of the profiles. It is pointed out that the lack of v_{rms} levels for ZDES mode 3 in the LES region near the RANS region is due to the attenuation of turbulent fluctuations provoked by the proximity of the RANS region. This attenuation is first observed in v_{rms}, and closer to the wall for u_{rms}. Such an observation is consistent with the profile of the resolved fraction of the Reynolds shear stress (figure 7).

Moreover, as already stated in the introduction, the resolved turbulence in the ZDES mode 3 allows for a more in depth analysis of the turbulence dynamics, which is the goal of the following section. The reader may find more details of the mean field profiles at different stations of wind tunnel in [3] for the same turbulence models.

4.3 Spectral assessment of Reynolds stresses

The satisfactory results from the ZDES mode 3 at the station presented in the previous section together with the feature of resolving part of the turbulence have encouraged to perform a spectral analysis of turbulence at that same station. In the outer layer, most of the turbulence is resolved by ZDES mode

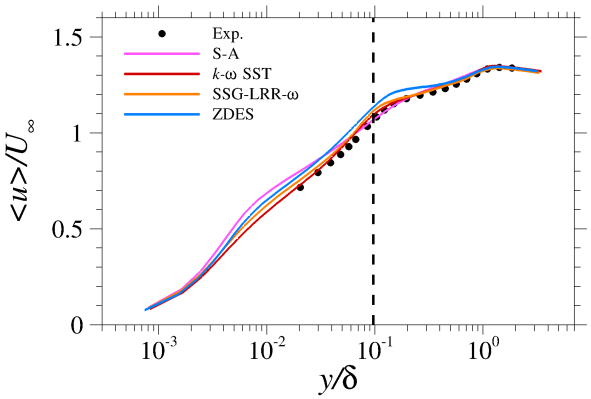

Fig. 4 Profile of mean velocity at $x/L = 10.73$. The dashed line corresponds to the position of the RANS/LES interface.

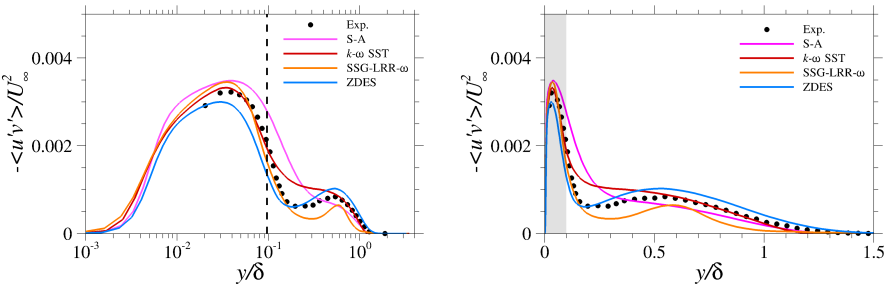

Fig. 5 Profile of the Reynolds shear stress in logarithmic scale (left) and in linear scale (right) at $x/L = 10.73$. The dashed line corresponds to the position of the RANS/LES interface and the shaded area represents the RANS region for the ZDES mode 3 simulation.

3. This is further evidenced in figure 7 which illustrates the resolved fraction of the Reynolds shear stress. It is clear from this figure, that in most of the LES region, the modelled contribution is negligible compared to the resolved Reynolds shear stress.

The power spectral density (PSD) of the streamwise velocity fluctuation and the premultiplied co-spectrum of the Reynolds shear stress as in equations (6) and (7) respectively are given in figures 8 and 9 for $\langle u'^2 \rangle$ and in figure 10 for $\langle u'v' \rangle$.

$$\langle u'^2 \rangle = \int_{-\infty}^{+\infty} k_x G_{uu}(k_x) \mathrm{d}\left(\ln(k_x)\right) \tag{6}$$

$$\langle u'v' \rangle = \int_{-\infty}^{+\infty} k_x G_{uv}(k_x) \mathrm{d}\left(\ln(k_x)\right) \tag{7}$$

where $G_{uv} = 2\mathrm{Re}(S_{uv})$, being S_{uv} the cross-PSD and $\mathrm{Re}(\bullet)$ the real part of a given quantity $(\bullet)$. It is noted that spectral analysis is performed using Welch's method [47] and Taylor's hypothesis of frozen turbulence for linking

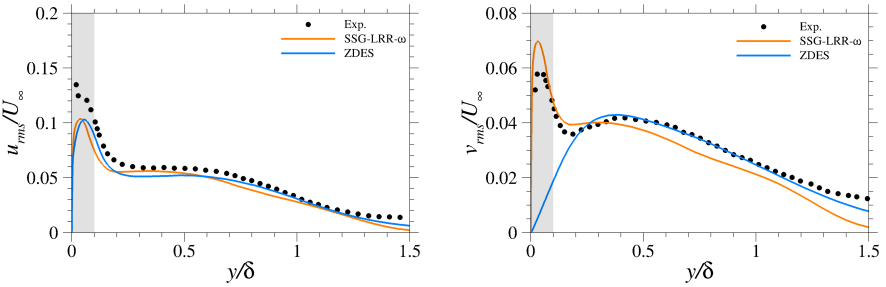

Fig. 6 Profiles of u_{rms} (left) and v_{rms} (right) at $x/L = 10.73$. The shaded area represents the RANS region for the ZDES mode 3 simulation.

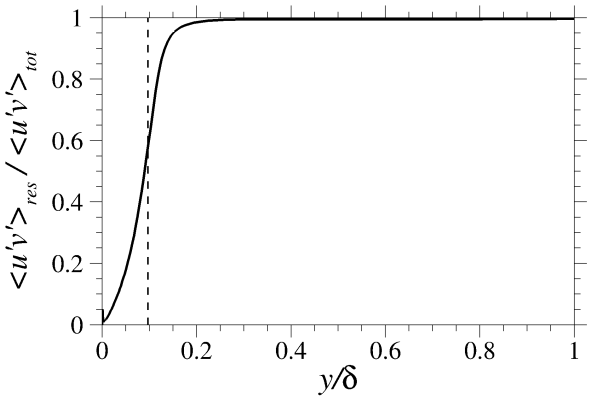

Fig. 7 Resolved fraction of the Reynolds shear stress in the ZDES mode 3 simulation at $x/L = 10.73$.

the frequency f (of a recorded time signal) with the streamwise wavelength $\lambda_x = U_c/f$. As a convection velocity, U_{corr} is employed, which is based on the two-point two-time correlation coefficient of streamwise velocity signals (see for instance [6, 48]). As stated in appendix A, U_{corr} is a good estimation of the local (wall distance dependent) convection velocity of turbulent structures.

The PSD of $\langle u'^2 \rangle$ is illustrated in figure 9 at a wall distance $d_w = 0.5\delta$. This is the location in the boundary layer where the outer peak of the Reynolds shear stress is observed (see figures 4 and 5). The PSD at this location confirms that turbulence is properly resolved by ZDES mode 3, since typical behaviours of the energy distribution appear to be reproduced, as suggested by the curves where the energy is proportional to k_x^{-1} and to $k_x^{-5/3}$ (see for instance [49]). Such an observation advocates that the turbulence in the outer layer is properly resolved regarding its physical dynamics. The extension of the regions showing the mentioned behaviours seems nevertheless limited, which may be explained by the Reynolds number not reaching sufficiently high values at the considered station ($Re_\theta \approx 4000$).

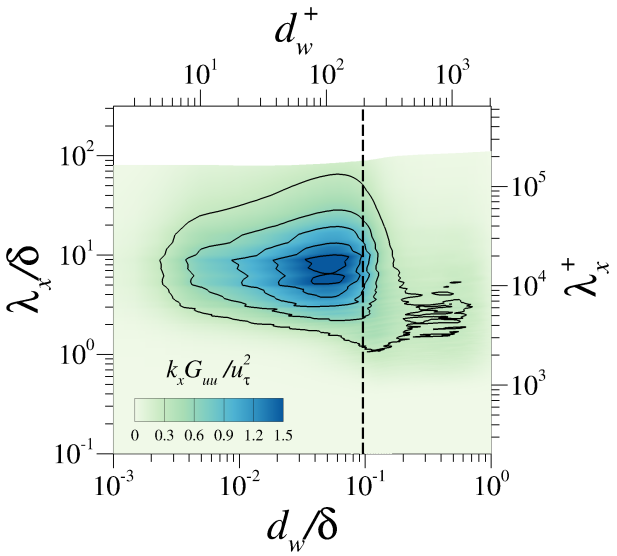

Fig. 8 Premultiplied power spectral density (PSD) of streamwise velocity fluctuations $k_x G_{uu}/u_\tau^2$. The dashed line corresponds to the position of the RANS/LES interface.

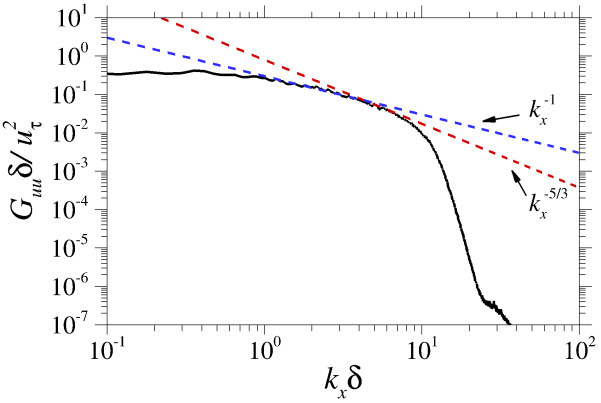

Fig. 9 Power spectral density of the streamwise velocity fluctuation at $x/L = 10.73$ and a wall distance $d_w = 0.5\delta$.

Moreover, in figures 8 and 10, it is interesting to notice a second region of energetic content in the streamwise velocity which is significantly more remarkable in the Reynolds shear stress and whose location corresponds to that of the external peak of the Reynolds shear stress profile. This energy is associated to structures of about 2δ to 3δ wavelength and therefore these structures are likely responsible for these unusual features found in the mean velocity and Reynolds shear stress profiles.

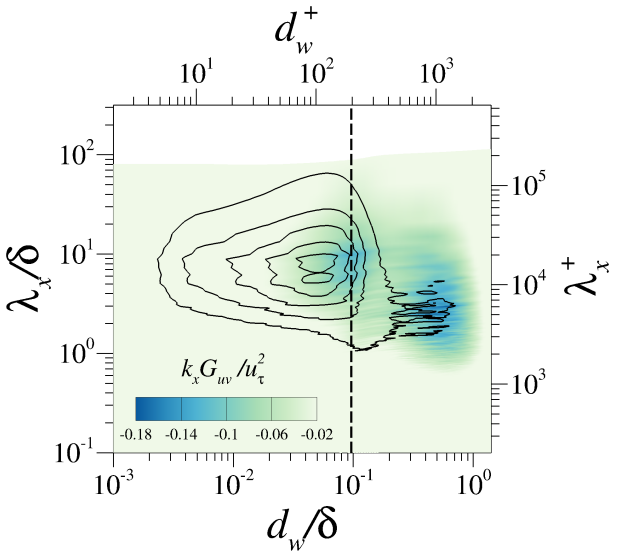

Fig. 10 Premultiplied co-spectrum of the Reynolds shear stress $k_x G_{uv}/u_\tau^2$. Black contours represent $k_x G_{uu}/u_\tau^2$. The dashed line corresponds to the position of the RANS/LES interface.

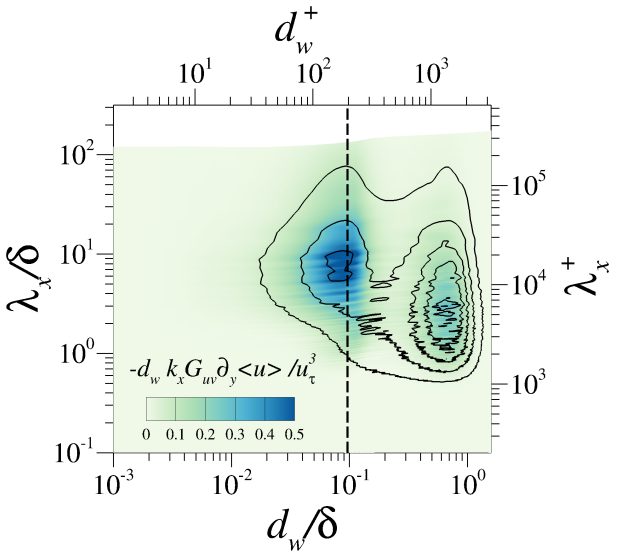

Fig. 11 PSD of the turbulent kinetic energy production term pre-multiplied by the wall distance $-d_w k_x G_{uv}/u_\tau^3\,(\partial\langle u\rangle/\partial y)$ at $x/L = 10.73$. Black contours represent $d_w k_x G_{uu}/(u_\tau^2 \delta)$. The dashed line corresponds to the position of the RANS/LES interface.

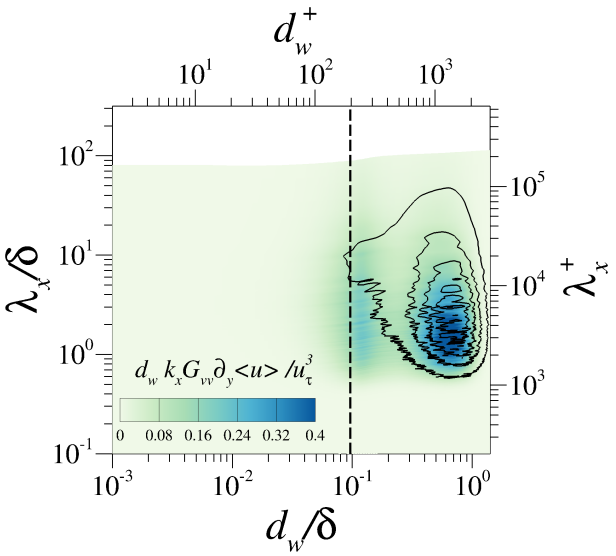

Fig. 12 PSD of the Reynolds shear stress production term pre-multiplied by the wall distance $d_w k_x G_{vv}/u_\tau^3\,(\partial\langle u\rangle/\partial y)$ at $x/L = 10.73$. Black contours represent $-d_w k_x G_{uv}/(u_\tau^2 \delta)$. The dashed line corresponds to the position of the RANS/LES interface.

Further spectral analysis is provided by figures 11 and 12, where the PSD of the production terms of the turbulent kinetic energy and of the Reynolds shear stress are presented. According to the boundary layer hypothesis, the production term of the turbulent kinetic energy transport equation reads [1, 50]:

$$\mathcal{P}_k = -\langle u'v' \rangle \frac{\partial \langle u \rangle}{\partial y} \tag{8}$$

which, considering equation (7), may be written as:

$$\mathcal{P}_k = -\int_{-\infty}^{+\infty} k_x G_{uv}(k_x) \frac{\partial \langle u \rangle}{\partial y} \mathrm{d}\left(\ln(k_x)\right). \tag{9}$$

The same reasoning leads to the following expression for the production term in the Reynolds shear stress transport equation:

$$\mathcal{P}_{-\langle u'v' \rangle} = \int_{-\infty}^{+\infty} k_x G_{vv}(k_x) \frac{\partial \langle u \rangle}{\partial y} \mathrm{d}\left(\ln(k_x)\right). \tag{10}$$

As observed in figures 11 and 12, there are again two clear energetic sites in the spectral content of the production terms. The outer site in both figures is located near the middle of the boundary layer, and is associated to turbulent structures of streamwise wavelengths from $\lambda_x \approx \delta$ up to $\lambda_x \approx 10\delta$, centred around $\lambda_x/\delta \approx 2-3$. Regarding the site located around 0.1δ away from the wall, slightly greater wavelengths are identified in the case of the turbulent

kinetic energy production. Another difference between the PSD of both production terms is observed in the intensity of both sites. The inner site is more energetic than the outer site for $\mathcal{P}_k$ (figure 11), whereas the opposite happens for $\mathcal{P}_{-\langle u'v'\rangle}$ (figure 12). Besides, for the latter, the energetic site near 0.1δ does not seem to correspond with energetic levels of the Reynolds shear stress. Further analysis of the Reynolds shear stress budget (not shown) has allowed to identify that there is an important local contribution of the mean-flow convection term, which compensates the production term up to 25%. Moreover, one could guess that there is a non-negligible contribution of the pressure term, since it is an important contributor in the Reynolds shear stress budget for zero-pressure-gradient turbulent boundary layers [1].

4.4 Evidence of two separated turbulent sites

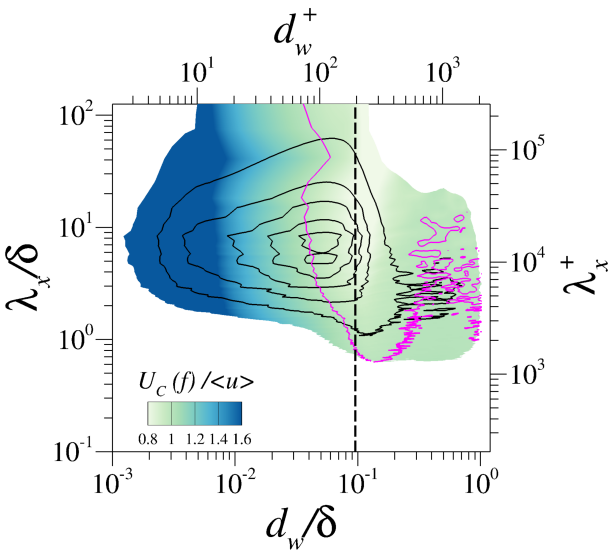

Fig. 13 Local frequency-dependent convection velocity normalised by the local mean velocity. Purple contours: loci of $U_c(f) = \langle u\rangle$. Black contours: $k_x G_{uu}/u_\tau^2$. The dashed line corresponds to the position of the RANS/LES interface.

The previous spectral analysis has allowed to identify that turbulent structures of wavelength λ_x between 2δ and 3δ strongly contribute to the dynamics of the outer peak observed in the Reynolds shear stress profile. In order to try to better comprehend the mechanisms underlying this peak, the convection velocity of u' dependent on the frequency, $U_c(f)$, is plotted in figure 13, normalized by the mean velocity $\langle u\rangle$. $U_c(f)$ is computed according to the work of [51], and it provides a convection velocity at each position of the boundary layer for the different turbulent scales involved, since Taylor's hypothesis

allows to link the frequency of the signal f and the wavelength λ_x. A reminder of the scale-dependent convection velocity is provided in appendix A.

As observed in figure 13, the convection velocity close to the wall is in overall significantly greater than the local mean velocity, which is in accordance with the results of [51]. Besides, Renard & Deck [51] found that near the three energetic sites in the PSD of $\langle u'^2 \rangle$ (for a WRLES simulation), the convection velocity was quite close to the local mean velocity. This can be seen as an analogy with the critical layer stability concept, which represents the loci where the phase velocity of a linear perturbation mode is equal to the mean velocity [52]. Such a result is also observed in figure 13 for both the inner ($d_w \approx 0.05\delta$) and outer ($d_w \approx 0.5\delta$) sites of G_{uu} obtained with ZDES mode 3. Therefore, the outer site observed in figures 8, 10, 11, 12 and 13, and responsible for the outer peak in the Reynolds shear stress, is a separated energetic site from the inner one, the latter being very close to the outer peak observed in zero-pressure-gradient turbulent boundary layers near the geometric centre of the logarithmic region (see [6]). Indeed, energy associated to high wavelengths closer to the wall in figure 8 may be seen as a footprint of structures located higher in the boundary layer, closer to the iso-line $U_c(f) = \langle u \rangle$ as also stated by [53]. Moreover, both sites have significantly different convection velocities, the one of the outer site being about 1.5 times greater than that of the inner site. It must be pointed out that the autonomy of both sites does not exclude the existence of an interaction between them, akin to what is observed for canonical zero-pressure-gradient turbulent boundary layers [54–56]. The identification of the outer site as independent from the inner site is a step towards better understanding the origin of this outer peak which is particular of this flow configuration since it is not observed in zero-pressure-gradient turbulent boundary layers [6, 11, 53–55].

The validity of Taylor's hypothesis may be assessed through the correlation coefficient as given by [51], which coincides with the dual case in [57], and it is denoted by γ_{cu} (see appendix A for details). This coefficient is plotted in figure 14 together with the PSD of the streamwise velocity fluctuation of figure 8. There is a decrease of the validity of Taylor's hypothesis with the increase of the structure wavelength, a result that has also been observed by [51] and complies with the analytical work of [58]. Indeed, for a given convection velocity, the time needed to traverse a distance corresponding to the streamwise wavelength of a coherent turbulent structure increases with the size of the mentioned structure. As a consequence, the convection time scale becomes less negligible against the time scale of evolution of large turbulent structures and hence, the validity of Taylor's hypothesis is reduced.

5 Conclusion

A turbulent boundary layer out of equilibrium at high Reynolds number has been assessed by means of ZDES mode 3. This approach allows to simulate this flow thanks to its important computational effort reduction compared to

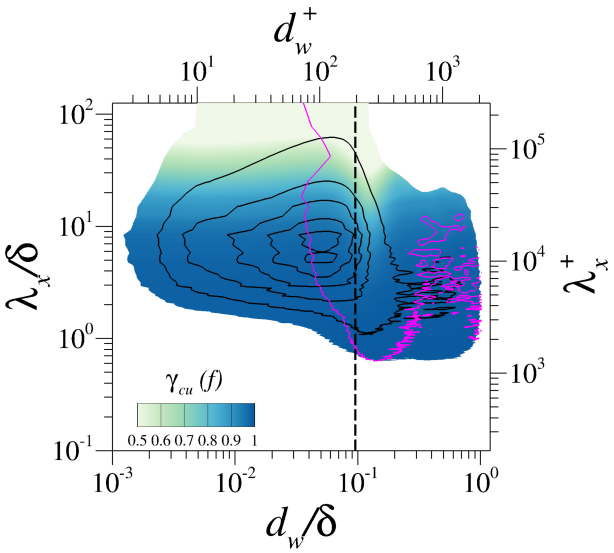

Fig. 14 Correlation coefficient γ_{cu}. Purple contours: loci of $U_c(f) = \langle u \rangle$. Black contours: $k_x G_{uu}/u_\tau^2$. The dashed line corresponds to the position of the RANS/LES interface.

WRLES and DNS, for which the resources required would probably not be affordable. Focus is made on a particular station for which the boundary layer is clearly out of equilibrium. These results point out the relevance of ZDES mode 3 compared to the RANS approach. Despite a greater numerical cost, resolving part of the turbulence allows to capture more physics of the flow therefore having a more reliable prediction of it. Mainly, the mean velocity excess and the Reynolds stresses profiles (which show an outer peak for $\langle u'v' \rangle$) are most satisfactorily predicted by ZDES mode 3 in terms of profile levels but specially in the terms of the profile trends. Indeed, eddy-viscosity models are not able to predict the outer peak of the Reynolds shear stress and the RSM models gives an outer peak of less intensity and narrower than the experimental measurements. More accurate results are obtained from the ZDES mode 3 simulation thanks to the resolved turbulence in the outer layer which allows to better take into account the non-canonical effects of the flow.

A spectral analysis of turbulence is achievable in the ZDES mode 3 computation which gives the possibility for more in depth turbulence studies. In particular in this case, thanks to turbulence spectral analysis, the unusual features observed in the profiles of mean velocity and Reynolds shear stress have been related to large turbulent structures associated to an energetic peak centred around wavelengths from 2 to 3 times the local boundary layer thickness. The spectral analysis of turbulence has been assessed in terms of the streamwise velocity fluctuation, the Reynolds shear stress as well as both the TKE and Reynolds shear stress production terms. The analysis of these two last terms has evidenced the contribution of very large turbulent structures of wavelengths reaching up to 10 times the local boundary layer thickness. It has also

led to consider the importance of other terms in the transport equations such as the advection term for the Reynolds shear stress. Furthermore, the assessment of the scale-dependent local convection velocity has permitted to identify that the structures linked to the outer peak compose a separated energy site in the outer part of the boundary layer, and they are convected significantly faster than structures belonging to the inner site. The validity of Taylor's hypothesis of frozen turbulence has also been discussed at this point thanks to the evaluation of the scale-dependent convection velocity and the correlation coefficient γ_{cu}. It has also been discussed the reduction of the validity of Taylor's hypothesis for structures of large wavelengths, compared to shorter coherent structures for which the correlation coefficient remains close to one.

Such in depth analysis of turbulence dynamics illustrates the potential of approaches such as ZDES mode 3 to finely describe turbulent flows in non-canonical conditions at high Reynolds numbers at an affordable computational cost. Moreover, such analysis contribute to the understanding of turbulence dynamics in out-of-equilibrium conditions and to highlight the universality of features observed in canonical conditions.

Acknowledgments. The authors are greatly thankful to all the people involved in the evolution of the FLU3M and elsA solvers. The authors would also like to express their gratitude to the committee of the *13th International ERCOFTAC symposium on engineering, turbulence, modelling and measurements, ETMM13* for encouraging this publication.

Appendix A Reminder about the scale-dependent convection velocity [51]

This appendix presents a reminder of the definition and evaluation of the convection velocity $U_c(f)$ of turbulent structures dependent on their streamwise length scale and, hence, on their frequency f, following the study of [51]. This convection velocity is studied in their work for a non-homogeneous mean flow in the streamwise direction, x, which is the case for instance in flat plate boundary layer flows. Their study is based on that of [57] made for channel flows, for which, on the contrary, the mean flow is homogeneous in the streamwise direction. The idea is to find a convection velocity $\mathcal{C}$ such that the residual of the advection equation is minimised :

$$\frac{1}{\mathcal{C}}\frac{\partial u'}{\partial t} + \frac{\partial u'}{\partial x} = 0. \tag{A1}$$

Thus, the global convection velocity, which takes into account the whole range of scales (or frequencies), $\mathcal{C}_u$, corresponds to that giving the minimum of the

quantity $\mathcal{D}(\mathcal{C})$, defined as:

$$\mathcal{D}(\mathcal{C}) = \frac{E\left[\left(\frac{1}{\mathcal{C}}\frac{\partial u'}{\partial t} + \frac{\partial u'}{\partial x}\right)^2\right]}{E\left[\left(\frac{\partial u'}{\partial x}\right)^2\right]} \tag{A2}$$

where $E[\bullet]$ denotes the mathematical expectation operator. Since the denominator of $\mathcal{D}(\mathcal{C})$ does not depend on $\mathcal{C}$, minimising either $\mathcal{D}(\mathcal{C})$ or $E\left[\left(\frac{1}{\mathcal{C}}\frac{\partial u'}{\partial t} + \frac{\partial u'}{\partial x}\right)^2\right]$ gives the same condition, which is:

$$\frac{\partial \mathcal{D}(\mathcal{C}_u)}{\partial \mathcal{C}} = 0 \Rightarrow \mathcal{C}_u = -\frac{E\left[\left(\frac{\partial u'}{\partial t}\right)^2\right]}{E\left[\frac{\partial u'}{\partial t}\frac{\partial u'}{\partial x}\right]}. \tag{A3}$$

Moreover, for $\mathcal{C}_u$ it is possible to rewrite (A2) such that:

$$1 - \gamma_{cu}^2 = \mathcal{D}(\mathcal{C}_u), \quad \gamma_{cu} \geq 0, \quad \Rightarrow \gamma_{cu} = \frac{|E\left[\frac{\partial u'}{\partial t}\frac{\partial u'}{\partial x}\right]|}{\sqrt{E\left[\left(\frac{\partial u'}{\partial t}\right)^2\right] E\left[\left(\frac{\partial u'}{\partial x}\right)^2\right]}} \tag{A4}$$

where γ_{cu} is a correlation coefficient ranging from 0 to 1 and corresponds to a validity indicator of Taylor's hypothesis of frozen turbulence ($\gamma_{cu} = 1$ in the case of perfect convection).

By considering the estimation of the PSD through Welch's method [47], as previously stated, together with some properties of the correlation functions [51, 59], one may write $\mathcal{C}_u$ as a function of the two-sided cross-PSD:

$$\mathcal{C}_u = \frac{-\int_{-\infty}^{+\infty} S_{\partial_t u \partial_t u;\, f}(f)\mathrm{d}f}{\int_{-\infty}^{+\infty} S_{\partial_t u \partial_x u;\, f}(f)\mathrm{d}f} = \frac{-\int_{-\infty}^{+\infty} (2\pi f)^2 S_{uu;\, f}(f)\mathrm{d}f}{\int_{-\infty}^{+\infty} -2i\pi f S_{u\partial_x u;\, f}(f)\mathrm{d}f} \tag{A5}$$

where $S_{\partial_t u \partial_t u;\, f}(f)$ represents the two-sided PSD of the temporal derivative of u' and $i^2 = -1$. It is possible to show that $S_{uu;\, f}(f)$ is a real function [59] and also that, for statistically stationary signals, $S_{uu;\, f}(f)$ is a symmetric function and therefore $S_{uu;\, f}(-f) = S_{uu;\, f}(f)$. It may also be written $S_{u\partial_x u;\, f}(-f) =$

$S^*_{u\partial_x u;\, f}(f)$ and thus:

$$\mathcal{C}_u = -\frac{\int_0^{+\infty} (2\pi f)^2 S_{uu;\, f}(f)\mathrm{d}f}{\int_0^{+\infty} 2\pi f\ \mathrm{Im}(S_{u\partial_x u;\, f}(f))\mathrm{d}f} \tag{A6}$$

where $\mathrm{Im}(\bullet)$ corresponds to the imaginary part. The expression for γ_{cu} may be then expressed as:

$$\gamma_{cu} = \frac{|\int_0^{+\infty} 2\pi f\ \mathrm{Im}(S_{u\partial_x u;\, f}(f))\mathrm{d}f|}{\sqrt{\int_0^{+\infty} (2\pi f)^2 S_{uu;\, f}(f)\mathrm{d}f}\sqrt{\int_0^{+\infty} S_{\partial_x u\partial_x u;\, f}(f)\mathrm{d}f}}. \tag{A7}$$

The final expressions for the convection velocity and the correlation coefficient as a function of the frequency (scale) $U_c(f)$ and $\gamma_{cu}(f)$ are obtained from equations (A6) and (A7) respectively by integrating in an infinitely small interval around a given frequency f_0 [51]:

$$U_c(f) = -\frac{2\pi f S_{uu;\, f}(f)}{\mathrm{Im}(S_{u\partial_x u;\, f}(f))}, \quad \gamma_{cu}(f) = \frac{|\mathrm{Im}(S_{u\partial_x u;\, f}(f))|}{\sqrt{S_{uu;\, f}(f)}\sqrt{S_{\partial_x u\partial_x u;\, f}(f)}}. \tag{A8}$$

In all the expressions here shown, the dependency on the wall distance has been omitted for clarity purposes. It is however important to remind that these expressions are given at a specified wall distance, so that for a given frequency there is a dependency of both $U_c(f)$ and $\gamma_{cu}(f)$ on the wall distance.

In [51], the convection velocity $U_c(f)$ and the correlation coefficient $\gamma_{cu}(f)$ are presented for a zero-pressure-gradient turbulent boundary layer at $Re_\theta = 13000$. The convection velocity is compared to the velocity based on the two-point two-time correlation U_{corr}, which is the one used in the present paper for the spectral analysis of turbulence. Quite close values between $U_c(f)$ and U_{corr} are obtained by [51] thus suggesting that U_{corr} is a good alternative for the convection velocity, since its computation is easier than that of $U_c(f)$. Indeed, U_{corr} may be seen as a weighted harmonic average of $U_c(f)$ [51], and is coincident with $\mathcal{C}_u$ (A6).

Declarations

- The thesis of J. Vaquero is partly funded by DGA (French defence procurement agency). Support from the framework of the ONERA research project FROTTEMENT is also acknowledged.
- The authors have no competing interests to declare that are relevant to the content of this article.

- All authors contributed to the study conception and design. Material preparation, data collection and analysis were performed by Jaime Vaquero under the supervision of Nicolas Renard and Sébastien Deck. The first draft of the manuscript was written by Jaime Vaquero and all authors commented on previous versions of the manuscript. All authors read and approved the final manuscript.

References

[1] Pope, S.B.: Turbulent flows. Cambridge University Press (2000)

[2] Sagaut, P., Deck, S., Terracol, M.: Multiscale and multiresolution approaches in turbulence. Imperial College Press (2013)

[3] Vaquero, J., Renard, N., Deck, S.: Advanced simulations of turbulent boundary layers under pressure-gradient conditions. Physics of Fluids **31**, 115111 (2019)

[4] Jiménez, J.: Computing high-Reynolds-number turbulence: will simulations ever replace experiments? Journal of Turbulence **4**, 22 (2003)

[5] Bannier, A., Garnier, É., Sagaut, P.: Riblet flow model based on an extended FIK identity. Flow, Turbulence and Combustion **95**, 351–376 (2015)

[6] Deck, S., Renard, N., Laraufie, R., Sagaut, P.: Zonal Detached Eddy Simulation (ZDES) of a spatially developing flat plate turbulent boundary layer over the Reynolds number range $3150 \leq Re_\theta \leq 14000$. Physics of Fluids **26**, 025116 (2014)

[7] Piomelli, U.: Wall-layer models for Large-Eddy Simulations. Progress in Aerospace Sciences **44**, 437–446 (2008)

[8] Deck, S.: Recent improvements in the Zonal Detached Eddy Simulation (ZDES) formulation. Theoretical and Computational Fluid Dynamics **26**, 523–550 (2012)

[9] Renard, N., Deck, S.: Improvements in Zonal Detached Eddy Simulation for Wall Modeled Large Eddy Simulation. AIAA Journal **53**, 3499–3504 (2015)

[10] Deck, S., Weiss, P.-E., Renard, N.: A rapid and low noise switch from RANS to WMLES on curvilinear grids with compressible flow solvers. Journal of Computational Physics **363**, 231–255 (2018)

[11] Deck, S., Renard, N., Laraufie, R., Weiss, P.-É.: Large-scale contribution to mean wall shear stress in high-Reynolds-number flat-plate boundary

layers up to $Re_\theta = 13650$. Journal of Fluid Mechanics **743**, 202–248 (2014)

[12] Spalart, P.R., Watmuff, J.H.: Experimental and numerical study of a turbulent boundary layer with pressure gradients. Journal of Fluid Mechanics **249**, 337–371 (1993)

[13] Skote, M., Henningson, D.S., Henkes, R.A.W.M.: Direct numerical simulation of self-similar turbulent boundary layers in adverse pressure gradient conditions. Flow, Turbulence and Combustion **60**, 47–85 (1998)

[14] Skote, M., Henningson, D.: Direct numerical simulation of a separated turbulent boundary layer. Journal of Fluid Mechanics **471** (2002)

[15] Cheng, W., Pullin, D.I., Samtaney, R.: Large-eddy simulation of separation and reattachment of a flat plate turbulent boundary layer. Journal of Fluid Mechanics **785**, 78–108 (2015)

[16] Kitsios, V., Sekimoto, A., Atkinson, C., Sillero, J.A., Borrell, G., Gungor, A.G., Jiménez, J., Soria, J.: Direct numerical simulation of a self-similar adverse pressure gradient turbulent boundary layer at the verge of separation. Journal of Fluid Mechanics **829**, 392–419 (2017)

[17] Bobke, A., Vinuesa, R., Örlü, R., Schlatter, P.: History effects and near equilibrium in adverse-pressure-gradient turbulent boundary layers. Journal of Fluid Mechanics **820**, 667–692 (2017)

[18] Tanarro, Á., Vinuesa, R., Schlatter, P.: Effect of adverse pressure gradients on turbulent wing boundary layers. Journal of Fluid Mechanics **883** (2020)

[19] Fan, Y., Atzori, M., Vinuesa, R., Gatti, D., Schlatter, P., Li, W.: Decomposition of the mean friction drag on an NACA4412 airfoil under uniform blowing/suction. Journal of Fluid Mechanics **932**, 31 (2021)

[20] Lee, J.H.: Large-scale motions in turbulent boundary layers subjected to adverse pressure gradients. Journal of Fluid Mechanics **810**, 323–361 (2017)

[21] Wenzel, C., Gibis, T., Kloker, M., Rist, U.: Self-similar compressible turbulent boundary layers with pressure gradients. Part 1. Direct numerical simulation and assessment of Morkovin's hypothesis. Journal of Fluid Mechanics **880**, 239–283 (2019)

[22] Park, J., Ha, S., You, D.: On the unsteady Reynolds-averaged Navier-Stokes capability of simulating turbulent boundary layers under unsteady adverse pressure gradients. Physics of Fluids **33**, 065125 (2021)

[23] Pozuelo, R., Li, Q., Schlatter, P., Vinuesa, R.: An adverse-pressure-gradient turbulent boundary layer with nearly constant $\beta \simeq 1.4$ up to $Re_\theta \simeq 8700$. Journal of Fluid Mechanics **939**, 34 (2022)

[24] Spalart, P., Allmaras, S.: A one-equation turbulence model for aerodynamic flows. La Recherche Aérospatiale, 5–21 (1994)

[25] Menter, F.R.: Two-equation eddy-viscosity turbulence models for engineering applications. AIAA Journal **32**, 1598–1605 (1994)

[26] Launder, B., Reece, G., Rodi, W.: Progress in the development of a Reynolds-stress turbulence closure. Journal of Fluid Mechanics **68**, 537–566 (1975)

[27] Speziale, C., Sarkar, S., Gatski, T.: Modelling the pressure–strain correlation of turbulence: an invariant dynamical systems approach. Journal of Fluid Mechanics **227**, 245–272 (1991)

[28] Cécora, R., Radespiel, R., Eisfeld, B., Probst, A.: Differential Reynolds-Stress Modeling for Aeronautics. AIAA Journal **53**, 739–755 (2015)

[29] Wilcox, D.: Turbulence Modeling for CFD. DCW Industries, La Cañada, Calif (2006)

[30] Deck, S., Weiss, P.-É., Pamiès, M., Garnier, E.: Zonal Detached Eddy Simulation of a spatially developing flat plate turbulent boundary layer. Computers & Fluids **48**, 1–15 (2011)

[31] Smagorinsky, J.: General circulation experiments with the primitive equations. Monthly weather review **91**, 99–164 (1963)

[32] Spalart, P.R., Jou, W.-H., Strelets, M., Allmaras, S.R.: Comments on the feasibility of LES for wings, and on a hybrid RANS/LES approach. *Proceedings of the First AFOSR International Conference on DNS/LES*, Greyden Press, 137–147 (1997)

[33] Renard, N., Deck, S.: Recent improvements in the formulation of mode III of ZDES (Zonal Detached Eddy Simulation) for WMLES use at $Re_\theta > 10^4$. *In 53rd AIAA Aerospace Sciences Meeting.* American Institute of Aeronautics and Astronautics (2015)

[34] Jarrin, N., Benhamadouche, S., Laurence, D., Prosser, R.: A synthetic-eddy-method for generating inflow conditions for large-eddy simulations. International Journal of Heat and Fluid Flow **27**, 585–593 (2006)

[35] Pamiès, M., Weiss, P.-E., Garnier, E., Deck, S., Sagaut, P.: Generation of synthetic turbulent inflow data for large eddy simulation of spatially

evolving wall-bounded flows. Physics of Fluids **21**, 045103 (2009)

[36] Laraufie, R., Deck, S.: Assessment of Reynolds stresses tensor reconstruction methods for synthetic turbulent inflow conditions. Application to hybrid RANS/LES methods. International Journal of Heat and Fluid Flow **42**, 68–78 (2013)

[37] Vaquero, J., Renard, N., Deck, S.: Outer layer turbulence dynamics in a high-Reynolds-number boundary layer up to $Re_\theta \approx 24{,}000$ recovering from mild separation. Journal of Fluid Mechanics **942**, 42 (2022)

[38] Vaquero, J., Renard, N., Deck, S.: Effects of upstream perturbations on the solution of the laminar and fully turbulent boundary layer equations with pressure gradients. Physics of Fluids **31**, 125103 (2019)

[39] Guillen, P., Dormieux, M.: Design of a 3D multidomain Euler code. Supercomputing in fluid flow, 21–39 (1993)

[40] Cambier, L., Heib, S., Plot, S.: The Onera elsA CFD software: input from research and feedback from industry. Mechanics & Industry **14**, 159–174 (2013)

[41] Cuvier, C., Srinath, S., Stanislas, M., Foucaut, J.M., Laval, J.P., Kähler, C.J., Hain, R., Scharnowski, S., Schröder, A., Geisler, R., Agocs, J., Röse, A., Willert, C., Klinner, J., Amili, O., Atkinson, C., Soria, J.: Extensive characterisation of a high Reynolds number decelerating boundary layer using advanced optical metrology. Journal of Turbulence **18**, 929–972 (2017)

[42] Liou, M.-S.: A sequel to AUSM: AUSM+. Journal of Computational Physics **129**, 364–382 (1996)

[43] Mary, I., Sagaut, P.: Large eddy simulation of flow around an airfoil near stall. AIAA Journal **40**, 1139–1145 (2002)

[44] Hunt, J., Wray, A., Moin, P.: Eddies, streams, and convergence zones in turbulent flows. *Proceedings of the Summer Program 1988*, Center for Turbulence Research (1988)

[45] Head, M.R., Bandyopadhyay, P.: New aspects of turbulent boundary-layer structure. Journal of Fluid Mechanics **107**, 297 (1981)

[46] Manceau, R.: Recent progress in the development of the Elliptic Blending Reynolds-stress model. International Journal of Heat and Fluid Flow **51**, 195–220 (2015)

[47] Welch, P.: The use of fast fourier transform for the estimation of power

spectra: A method based on time averaging over short, modified periodograms. IEEE Transactions on Audio and Electroacoustics **15**, 70–73 (1967)

[48] Dennis, D.J.C., Nickels, T.B.: On the limitations of Taylor'shypothesis in constructing long structures in a turbulent boundary layer. Journal of Fluid Mechanics **614**, 197–206 (2008)

[49] Perry, A.E., Henbest, S., Chong, M.S.: A theoretical and experimental study of wall turbulence. Journal of Fluid Mechanics **165**, 163 (1986)

[50] Cousteix, J.: Turbulence et Couche Limite. Cepadues-éditions, Toulouse (1989)

[51] Renard, N., Deck, S.: On the scale-dependent turbulent convection velocity in a spatially developing flat plate turbulent boundary layer at Reynolds number $Re_\theta = 13000$. Journal of Fluid Mechanics **775**, 105–148 (2015)

[52] Charru, F.: Hydrodynamic Instabilities. Cambridge University Press, Cambridge New York (2011)

[53] Renard, N., Deck, S.: On the convection velocity of wall-bounded turbulence resolved by ZDES mode III at $Re_\theta = 13000$. *In Progress in Hybrid RANS-LES Modelling*. Springer International Publishing, 325–336 (2018)

[54] Mathis, R., Hutchins, N., Marusic, I.: Large-scale amplitude modulation of the small-scale structures in turbulent boundary layers. Journal of Fluid Mechanics **628**, 311–337 (2009)

[55] Smits, A.J., McKeon, B.J., Marusic, I.: High Reynolds number wall turbulence. Annual Review of Fluid Mechanics **43**, 353–375 (2011)

[56] Ganapathisubramani, B., Hutchins, N., Monty, J.P., Chung, D., Marusic, I.: Amplitude and frequency modulation in wall turbulence. Journal of Fluid Mechanics **712**, 61–91 (2012)

[57] del Álamo, J.C., Jiménez, J.: Estimation of turbulent convection velocities and corrections to Taylor's approximation. Journal of Fluid Mechanics **640**, 5–26 (2009)

[58] Lin, C.: On Taylor's hypothesis and the acceleration terms in the Navier-Stokes equations. Quarterly of Applied Mathematics **10**, 295–306 (1953)

[59] Bendat, J.S., Piersol, A.G.: Random data: Analysis and measurement procedures. 4th edn. Wiley (2010)